JOURNAL OF GEOPHYSICAL RESEARCH, VOL. 98, NO. C9, PAGES 16,529–16,546, SEPTEMBER 15, 1993

Open Boundary Conditions for the Extended Kalman Filter With a Quasi-Geostrophic Ocean Model

GEIR EVENSEN

Nansen Environmental and Remote Sensing Center, Bergen, Norway

The formulation of consistent boundary conditions for the quasi-geostrophic (QG) model with an extended Kalman filter in a data assimilation scheme is discussed. To form a well-posed boundary value problem for the QG model, the stream function must be specified at all boundaries and the vorticity must be specified at the inflow boundaries. The situation becomes significantly more complicated when proper boundary conditions are to be specified for the error covariance evolution equation. For closed or periodic boundaries no severe problems occur, but in general cases with open boundaries, only approximative methods can be used. Here a scheme is presented which allows for the stream function to be updated on the boundaries, e.g., from the use of measurements located close to the boundaries, or from meanders and eddies approaching the boundaries from the interior of the domain. Further, the boundary value problem for the error covariance evolution equation is treated extensively. It is demonstrated that numerical discretization of the error covariance evolution equation leads to severe numerical difficulties when open boundaries are used. An approximate numerical scheme that can be used to handle open boundaries with inflow and outflow is proposed, and examples are given to illustrate the method. Is is shown that the boundary scheme is consistent and can be used even with data located at inflow boundaries. However, the approximations used in the scheme may lead to loss of positive definiteness for the error covariance matrix and an algorithm must be used to ensure positive definiteness for long time integrations.

INTRODUCTION

As given by *Evensen* [1992] (hereafter called Part I), the general formulation of the extended Kalman filter with a multilayer quasi-geostrophic (QG) model was discussed. Further, data assimilation experiments were performed on a square domain, using closed boundary conditions. One of the main topics considered was the instability connected to the linearization in the error covariance evolution equation. In this paper the work in Part I is extended to include open boundaries with inflow and outflow. The use of inflow boundaries with the QG model severely complicates the numerical treatment, but it is also of vital importance if mesoscale circulation is to be studied, using an extended Kalman filter to assimilate data in the QG model.

Open and closed boundaries have quite different properties and are normally treated differently in a way that leads to a well-posed problem. It should be remembered that an open boundary with inflow or outflow is an artificial boundary. No knowledge is therefore available about how an open boundary shall be updated unless external data or information can be used.

The general boundary conditions for the QG model have been discussed in several publications where *Charney et al.* [1950] gave the first consistent formulation resulting in a well-posed problem. Their main result is that the stream function must be specified on all boundaries to solve a well-posed Helmholtz problem. Further, the vorticity must be specified on the inflow boundaries.

When the extended Kalman filter is used for data assimilation with the QG model, two important issues must be considered.

Paper number 93JC01365.
0148–0227/93/92JC–01365$05.00

1. The Kalman filter will change an inflow boundary if measurements are located close to the boundary. A boundary scheme which allows for changes in the stream function, caused by assimilation of measurements located close to the inflow boundaries, is therefore needed.

2. An implementation of stable and consistent open boundary conditions for the error covariance evolution equation is required. This is a nontrivial problem as will be illustrated in the later sections.

Here an approximate but stable method is proposed which estimates the vorticity on all the boundaries using the same scheme independent of the type of boundary. It allows for the inflow boundary stream function to be changed during the time integration, either by wave structures propagation out through the boundary from the interior domain when a radiation condition is used, or by the assimilation of measurements using the Kalman filter.

The specific formulation of the boundary value problem for the error covariance evolution equation in connection with the QG model has not previously been discussed in the literature, except for the work by *Miller* [1986], who examined the Kalman filter with a one-dimensional linear barotropic QG model with open boundary conditions for Rossby wave propagation. However, he did not give any specific explanation of how the open boundary value problem for the error covariance evolution was handled. Here the problem is further complicated by the inclusion of advection and nonlinear physics.

The use of open inflow boundaries for the QG model introduces additional effects than what would be expected from the use of the pure ocean model. Here it is shown that an approximate algorithm can be used for the boundary conditions for the error covariance evolution equation. Several examples are given to illustrate its properties.

First, the equations for the multilayer QG model are given in the next section followed by a discussion of the boundary

conditions and the boundary vorticity schemes for the QG model. Then the formulation of consistent boundary conditions for the error covariance evolution is treated, and an approximate but stable scheme is proposed. Some examples where the proposed scheme is applied in a data assimilation experiment with open boundaries are then discussed, and finally the conclusions are given.

EQUATIONS FOR THE LAYERED MODEL

The ocean model is multilayered and describes conservation of potential vorticity ζ_l in each layer on an f plane. The mean layer thicknesses are D_l, and the density in each layer is ρ_l, where l denotes layer number; $l = 1$ in the upper layer. Ψ_l is the stream function in layer l. The horizontal length scale R_d is the internal Rossby radius of deformation of the upper layer, given by $R_d^2 = [(\rho_2 - \rho_1)gD_1] / \left[\rho_0 f^2\right]$, where g is the gravitational acceleration, ρ_0 is averaged density and f is the Coriolis parameter. The characteristic horizontal velocity is denoted U, yielding a time scale $T = R_d/U$. The pressure scale is $\rho_0 f U R_d$, and the stream function scale is $U R_d$. The nondimensional quasi-geostrophic equations [see *Pedlosky*, 1987] are

$$(\frac{\partial}{\partial t} + u_l \frac{\partial}{\partial x} + v_l \frac{\partial}{\partial y})\zeta_l = 0, \quad l = 1, n_z, \tag{1}$$

where n_z is the number of layers and the velocities are the geostrophic approximations

$$u_l = -\frac{\partial \Psi_l}{\partial y} \qquad v_l = \frac{\partial \Psi_l}{\partial x}. \tag{2}$$

The vorticity in each layer is given by

$$\zeta_1 = \nabla^2 \Psi_1 + fr_{1,2}(\Psi_2 - \Psi_1), \tag{3a}$$

$$\zeta_l = \nabla^2 \Psi_l - fr_{l,1}(\Psi_l - \Psi_{l-1}) + fr_{l,2}(\Psi_{l+1} - \Psi_l), \text{ for } l = 2, n_z - 1, \tag{3b}$$

$$\zeta_{n_z} = \nabla^2 \Psi_{n_z} - fr_{n_z,1}(\Psi_{n_z} - \Psi_{n_z-1}) + \eta, \tag{3c}$$

which constitutes a set of Helmholtz equations for Ψ when ζ is known. The Laplacian is $\nabla^2 = \partial^2/\partial^2 x + \partial^2/\partial^2 y$, and the constants $fr_{l,1}$ and $fr_{l,2}$ are "nondimensional Froude numbers"

$$fr_{l,1} = \frac{D_1}{D_l} \frac{\rho_2 - \rho_1}{\rho_l - \rho_{l-1}} \tag{4}$$

$$fr_{l,2} = \frac{D_1}{D_l} \frac{\rho_2 - \rho_1}{\rho_{l+1} - \rho_l}. \tag{5}$$

The bottom topography term is

$$\eta = \varepsilon^{-1} \frac{h}{D_{n_z}}, \tag{6}$$

with ε as the Rossby number and h as bottom topography. The QG model was further discussed in Part I.

BOUNDARY CONDITIONS FOR THE QG MODEL

As an introduction to the further discussion, note the following rather obvious points:

1. In the QG model the potential vorticity is advected along the streamlines (which are lines with constant stream function values).

2. A closed boundary will have a constant stream function along the boundary; i.e., closed boundaries can be streamlines. Variation of the stream function along a boundary determines whether there is inflow or outflow, dependent on the sign of the derivative of the stream function along the boundary.

3. The fact that the stream function is constant along the streamlines significantly simplifies the specification of proper boundary conditions for the QG model. Unless external specifications of the boundary stream function (e.g., estimating boundary conditions from a large-scale model), or radiation conditions are used, the boundary stream function will always remain constant in time.

The simplest case is to use closed boundaries. Then the normal velocities at the boundaries are zero, and also very small at the grid points next to the boundaries. A one-dimensional advection scheme can then be used for the grid points next to the boundaries and the specification of boundary vorticity is avoided.

The vorticity next to an outflow boundary can be updated using an upstream scheme and the specification of the boundary vorticity is avoided. The accuracy of this scheme is not crucial because most of the errors are advected out of the domain.

As stated above, the vorticity at the inflow boundaries must be specified in order to formulate a well-posed problem. In most cases there will not be any external data available for the vorticity at the inflow boundaries. It must therefore be specified based on assumptions about the structure of the stream function outside the boundary. A certain accuracy when calculating the vorticity at the inflow boundaries is important because the vorticity is advected directly into the model domain where it will influence the solution.

It would simplify the treatment of the boundaries if the same advection scheme could be used for all the internal grid points. If a 9-point advection formula is used, the vorticity must be specified on all boundaries, both open and closed, because the boundary vorticity is used when the vorticity at grid points next to the boundaries are updated. A method that can be used to specify the boundary vorticity with good enough accuracy on all types of boundaries and in a way that is stable on inflow boundaries is then needed. This is nontrivial because the relative vorticity term $\nabla^2\Psi$ requires knowledge of stream function values outside the numerical grid to specify the boundary vorticity when a centered difference scheme is used. Further, the use of stream function values in the interior domain to extrapolate the inflow boundary vorticity, is unstable in many cases. Note, however, that such a method can be used in connection with a radiation condition for the stream function, as will be illustrated.

In the previous works by *Haugan et al.* [1989, 1991] and *Ikeda et al.* [1989] where inflow boundaries were used, this was in connection with a jet propagating through the domain. In these works the inflow vorticity was specified once, using an assumption on the stream function outside the boundary, and thereafter kept constant during the run. This is a valid assumption as long as the stream function does not change at the grid points next to the boundary, and it is therefore not possible to handle meanders in the jet which approach the inflow boundary and change the boundary vorticity.

The goal of this section is to find a method for estimating the boundary vorticity, where the method is independent of the type of boundary. With such a scheme, the boundary

vorticity is estimated at all boundaries, and the same advection operator can be used for all the internal grid points. Further, the stream function is allowed to change at the boundaries. First, a simple radiation condition is presented and then two boundary vorticity schemes are discussed.

Radiation Condition

A radiation condition is based on the assumption that waves in the computational domain are propagating toward the boundaries with a given phase velocity. For a one-dimensional domain, these waves can be described by an advection equation

$$\frac{\partial \Psi}{\partial t} + c\frac{\partial \Psi}{\partial x} = 0, \tag{7}$$

where c is the phase velocity of the wave. A simple radiation condition has been used for the QG model, where the waves are assumed to propagate normal to the open boundaries with the phase velocity of the fastest growing wave predicted by linear stability theory [see *Ikeda and Lygre*, 1989]. The boundary stream function is then updated using an upstream difference scheme for (7).

First Boundary Vorticity Scheme

The first scheme is based on the standard assumption that the inflow boundary vorticity is specified once and thereafter used in all later time steps. This will of course imply a loss of flexibility because the inflow boundaries must be kept constant in time. They can not be updated by external data through the Kalman filter equations, or by radiation conditions. An advantage is that no instabilities occur and the accuracy is high, as long as no meanders or eddies approach the inflow boundary.

In the general case, the inflow vorticity must be stored throughout the integration of the model. However, if the inflow boundary is determined from a jet that is normal to the boundary, an alternative scheme can be used, because the cross-boundary variation of the stream function vanishes. It is based on the assumption that the contribution to the vorticity from cross-boundary variation of the stream function is small, i.e.,

$$\left.\frac{\partial^2 \Psi}{\partial x^2}\right|_{x=0} = 0, \tag{8}$$

where x is interpreted as the component normal to the boundary. The relative vorticity at all boundary points is then approximated solely from the variation of the stream function along the boundary, plus the contribution from the interaction terms between the layers and the bottom topography. The consequences of this assumption are that the flow must be normal to the boundary and at the same time it can not have any curvature at the boundary. Under these constraints equation (8) will be valid and the relative vorticity term may be calculated without references to the stream function outside the grid. With the specification of the stream function at the inflow boundaries the vorticity is also specified because it only refers to stream function values at the boundary points.

In the case of a jet which is normal to the boundary, this scheme is exact and identical to the specification of a constant boundary vorticity, as discussed above. In addition, it is possible to use a radiation condition to update the stream function on the inflow boundary.

The scheme can actually be used for all boundaries in the ocean model. At a closed boundary, Ψ is constant and all derivatives along the boundary are equal to zero. With the assumption in equation (8) the relative vorticity becomes zero and is neglected at the closed boundaries. This represents no constraint on the flow tangential to the boundary because no restriction has been applied to the first derivative of Ψ normal to the boundary. The errors resulting from using this scheme on the closed boundaries are negligible because the contribution from the boundary vorticity in the advection scheme is small. The vorticity at the outflow boundaries is advected out of the domain, and the influence on the internal domain has been negligible in the case studies presented in this paper.

Second Boundary Vorticity Scheme

The probably best approximation of the boundary vorticity is obtained by using a one-sided finite difference formula for the second derivative in the direction normal to the boundary. A second-order formula in Δx should be used to give the same accuracy as in the internal domain, and it is given as

$$\left.\frac{d^2 \Psi}{dx^2}\right|_0 = \frac{2\Psi_0 - 5\Psi_1 + 4\Psi_2 - \Psi_3}{\Delta x^2} + O(\Delta x^2). \tag{9}$$

If this formula is used for the inflow boundaries, it will lead to instabilities. The reason for this is that the internal stream function, which is partially determined from the boundary vorticity which has propagated into the domain, is recursively used to determine the new boundary vorticity. Fortunately, this instability can be avoided if a radiation condition is used for the stream function on the inflow boundaries.

Examples

The boundary vorticity schemes will now be illustrated using a simple example, where a barotropic cyclone on a sloping bottom is interacting with a jet propagating through a domain. This case is based on the examples from *Ikeda and Lygre* [1989], who studied eddy–jet interactions with the QG model.

The following parameters have been used in all the model runs: The internal Rossby radius is $R_d = 5835$ m, and the nondimensional grid spacing is $\Delta x = 0.5$. The velocity scale $U = 0.3$ m s^{-1}, and the nondimensional time step is calculated from the stability condition; typically, $\Delta t = 0.5$. The total depth is 300.0 m and an upper layer of 50.0 m and a lower layer of 250.0 m have been used with a density difference of $\Delta\rho = 1.0$ kg m^{-3}. This results in Froude numbers $fr_{1,2} = 1.0$ and $fr_{2,1} = 0.2$, and using a Coriolis parameter $f = 1.25 \times 10^{-4}$, the Rossby number becomes $\varepsilon = U/fR_d \simeq 0.41$. These parameters are typical for mesoscale processes in the Norwegian coastal waters. The QG model has proven to give good results in this parameter regime as discussed by *Haugan et al.* [1991] and *Ikeda et al.* [1989], even though the Rossby number is quite large.

First, a base case is created, where the initial upper layer stream function is defined by a jet with a Gaussian velocity profile that propagates through the domain, and is interacting with a barotropic cyclonic eddy. A 75×41 grid is used.

The jet is initialized as

$$\Psi_1 = -0.8 \int_0^y \exp\left[-\left(\frac{y'-5}{2}\right)^2\right] dy', \qquad (10)$$

$$\Psi_2 = 0.0,$$

and then the barotropic cyclone is added in both layers,

$$\Psi_l = \Psi_l - 2\exp\left[-\left(\frac{\sqrt{(x-12.5)^2+(y-8.5)^2}}{2}\right)^2\right], \qquad (11)$$

for $l = 1, 2$. The bottom topography is assumed to be

$$h(x) = \begin{cases} 25 \text{ m}, & \text{for } x < 5.00, \\ -\frac{50}{15}(x-12.5) \text{ m}, & \text{for } 5.0 < x < 20.0, \\ -25 \text{ m}, & \text{for } x > 20.0. \end{cases} \qquad (12)$$

This causes the eddy to propagate along the bottom slope and into the jet. The boundaries at $y = 0$ and $y = 20$ are treated as closed and the stream function is constant in time. At the outflow boundary $x = 37$, a radiation condition is used for the stream function.

Now four cases are run, where the purpose is to demonstrate how the vorticity can be updated on an inflow boundary when the stream function at the boundary or close to the boundary is altered, e.g., by using the Kalman filter, or, as in the cases given here, when structures are propagating towards the inflow boundary. The cases are:

Case O1. The first boundary scheme with the assumption (8) is used, with no radiation condition on the inflow boundary.

Case O2. The first boundary scheme with the assumption (8) is used, including a radiation condition on the inflow boundary.

Case O3. The second boundary scheme, where the variation normal to the boundary is calculated using the one-sided difference formula (9), and with no radiation condition on the inflow boundary.

Case O4. The second boundary scheme, where the variation normal to the boundary is calculated using the one-sided difference formula (9), including a radiation condition on the inflow boundary. All case studies performed in this paper are listed in Table 1.

In case O1 (Figure 1) the anticyclone on the inside of the jet is trapped in the corner between the inflow boundary and the closed boundary, and it is obvious that it strongly affects the stream function field close to the inflow boundary. In real life the anticyclone should propagate out of the domain, through the open inflow boundary.

In case O2 (Figure 2) the same vorticity scheme as in case O1 has been used, but a radiation condition has now been applied at the inflow boundary. This makes it possible for the eddy to propagate through the inflow boundary, and it disappears from the domain. The bad structures that were caused by the eddy at the inflow boundary are also removed. Note that the axis of the jet (thick line) is also changing slightly at the boundary, i.e., the boundary stream function is changing and the boundary vorticity is updated accordingly. By using this scheme it is now possible to alter the stream function on the inflow boundaries.

In case O3 (Figure 3) the second boundary scheme has been used, where the cross-boundary variation of the stream function is calculated by the one-sided difference formula (9). This scheme proves to be unstable, although the one-sided difference formula gives a better estimate of the cross boundary variation than just setting it to zero as in the first scheme. In this case the boundary vorticity is propagating into the domain where it affects the stream function, which is repeatedly used to estimate the new boundary vorticity. Errors in the boundary vorticity will then accumulate and cause the instability to grow. In the cases shown here a Shapiro filter of order 8 has been used every time step (see the discussion in Part I). The filter is damping the instability because the strong gradients close to the inflow boundary are smoothed, and the instability will grow faster without the use of the Shapiro filter.

In case O4 (Figure 4) the second boundary scheme has been used together with a radiation condition for the stream function. In this case the scheme is stable and the results are quite similar to case O2, except that the anticyclone seems to use longer time to escape the domain. It is hard to say if the results from this case are worse or better than the results in case O2.

The accuracy of these schemes should also be tested for closed and outflow boundaries, to compare their performance on more general cases, but that will not be done in this paper. The main conclusion from these examples is that both schemes can be used together with a radiation condition which updates the stream function on the inflow boundary. This result also suggests that the schemes should work in the case when the boundary stream function is changed by the assimilation of measurements.

Error Covariance Evolution Equation

The evolution of the error covariances is calculated using the tangent linear operator of the model. For a linear model this is equivalent to using the model advection matrix. For a nonlinear model the linearized advection operator taken at the current state estimate gives the tangent linear operator.

The discretized QG model was in Part I given on the form

$$L\boldsymbol{\psi}_{k+1} = \mathbf{f}(\boldsymbol{\psi}_k). \qquad (13)$$

Here the matrix L is the elliptic operator resulting from discretizing the system of Helmholtz equations (3), and with one on the diagonal in rows which corresponds to boundary points. The nonlinear vector function $\mathbf{f}(\boldsymbol{\psi}_k)$ contains in elements corresponding to internal grid points the advected potential vorticity with the bottom topography term subtracted. In elements corresponding to the boundary points, it contains the boundary conditions for the stream function.

The error covariance equation for the QG model was

$$LP_{k+1}L^T = F_k P_k F_k^T + LQ_{k+1}L^T. \qquad (14)$$

The tangent linear operator, or transition matrix F_k is the Jacobi matrix of the vector function $\mathbf{f}(\boldsymbol{\psi}_k)$, taken at the current stream function estimate. The part of F_k that corresponds to internal grid points can be written as

$$F_k' = \left[\Gamma(\boldsymbol{\psi})L'' + \frac{\partial\Gamma(\boldsymbol{\psi})}{\partial\boldsymbol{\psi}}(L''\boldsymbol{\psi} + \boldsymbol{\eta})\right]_{\boldsymbol{\psi}=\boldsymbol{\psi}_k^{\mathrm{a}}}, \qquad (15)$$

where $\boldsymbol{\psi}_k^{\mathrm{a}}$ is the analyzed stream function estimate at time t_k. The matrix $\Gamma(\boldsymbol{\psi})$ is the nonlinear advection operator used in the QG model, and it generates the updated covariance vorticity for the internal grid points. The matrix L'' is the Helmholtz operator and generates the potential vortic-

TABLE 1. Case Studies

	Ocean Model Runs	
	Cross-Bnd. Variation	Radiation Cond.
Case O1	Neglected	No
Case O2	Neglected	Yes
Case O3	One sided	No
Case O4	One sided	Yes
Error Covariance Runs		
Case E1	Uniform error field	
Case E2	Low errors on closed and outflow boundaries	
Case E3	Low errors on all boundaries	
Data Assimilation Experiments		
Experiment A	Stream through a channel, jet initialized	
Experiment B	Stream along coast, no jet initialized	

The case studies consists of four cases (O1–O4) where the inflow boundary vorticity schemes (8) and (9) are demonstrated for the ocean model, with and without radiation conditions on the inflow boundary. Three cases (E1–E3) have been run to verify the inflow boundary method for the error covariance equation. Finally, two data assimilation experiments (A and B) have been run to examine the proposed method in practical use.

ity. The double prime denotes that it contains schemes for the boundary vorticity at rows corresponding to boundary points. This operator was discussed in detail in Part I. The first term describes pure evolution of the error covariance vorticity in the model estimated velocity field, i.e., first L'' is operated on the covariance functions to generate the covariance vorticities, and these are then advected using the operator $\Gamma(\psi)$. The second term contains the additional effects of the nonlinearity in the QG model, like the local error growth discussed in Part I. The matrix Q_k is the error covariance matrix for the system noise.

The error covariance evolution equation (14) can be written as

$$P_{k+1} = L^{-1}F_k(L^{-1}F_kP_k)^T + Q_{k+1}. \tag{16}$$

This equation is solved by performing the following steps:

1. Calculate the matrix-matrix multiplication $P_a = F_kP_k$. The matrix P_a then contains the advected covariance vorticity.

2. Solve the elliptic systems $LP_b = P_a$. This results in intermediate covariance functions.

3. Calculate the matrix-matrix multiplication $P_c = F_kP_b^T$. The advected vorticity of the intermediate covariance functions is then contained in P_c.

4. Solve the elliptic systems $LP_d = P_c$. This results in the error covariance matrix in time step t_{k+1} before the system noise is added.

5. Add the system noise, $P_{k+1} = P_d + Q_{k+1}$.

The first step requires the covariance vorticity to be specified on the inflow boundaries to formulate a well-posed problem. This can be done using the one-sided difference formula (9). Note that the condition (8) which assumes that the cross-boundary variation is zero, can not be used, because this assumption is positively wrong for the covariance functions. However, scheme (9) gives a consistent estimate of the boundary covariance vorticity.

In step two, an intermediate covariance matrix is solved for, and boundary conditions for all the intermediate covariance functions are required. This is a nontrivial problem, when inflow boundaries are present, because it requires information about the covariance function outside the inflow boundary. Figure 5 illustrates how a covariance function at a grid point close to the inflow boundary, in a uniform flow, leads to an intermediate covariance function that is advected with the flow. It is the estimate of the inflow boundary conditions of this intermediate covariance function which causes the problems. Note that this problem arises because the equations are discrete in time.

In step three, the vorticity of the intermediate covariance functions must be specified at the inflow boundaries. This can also be done using the scheme (9).

In the fourth step, the final covariance functions are solved for and boundary conditions are required on all boundaries. It is natural to use the boundary values from the previous time step for the inflow and closed boundaries. On the outflow boundaries, a radiation condition might be used.

Estimate of the Intermediate Boundary Covariance

An approximate method is needed to estimate boundary conditions for the intermediate covariance functions. The boundary scheme must use an estimate of the covariance function outside the inflow boundary, to calculate an approximation for the intermediate covariance functions on the boundary. The estimate of the covariance function outside the inflow boundary can be calculated using an extrapolation method. A Taylor expansion about the boundary point (denoted with subscript 0),

$$p_{-1} = p_0 - \left.\frac{dp}{dx}\right|_0 \Delta x + \left.\frac{1}{2}\frac{d^2p}{dx^2}\right|_0 \Delta x^2 + O(\Delta x^3), \tag{17}$$

has been used, where the p_{-1} is the covariance value in a grid point located a distance Δx outside the boundary in negative x direction. A one-dimensional formula is used to illustrate the scheme, but a multidimensional case, such as the multilayer QG model, does not introduce any additional problems. The derivatives must be estimated using finite difference approximations. Several extrapolation formulas can be generated by choosing different alternative difference approximations for the first and second derivatives. Here both centered and one-sided second-order formulas have been tested. For the first derivative these are the centered formula

$$\left.\frac{dp}{dx}\right|_0 = \frac{p_1 - p_{-1}}{2\Delta x} + O(\Delta x^2), \tag{18}$$

and the one-sided formula

$$\left.\frac{dp}{dx}\right|_0 = \frac{-1.5p_0 + 2p_1 - 0.5p_2}{\Delta x} + O(\Delta x^2). \tag{19}$$

For the second derivative the centered formula is

$$\left.\frac{d^2p}{dx^2}\right|_0 = \frac{p_1 - 2p_0 + p_{-1}}{\Delta x^2} + O(\Delta x^2), \tag{20}$$

and the one-sided formula is given by (9).

If the one-sided formulas, (18) and (9), are used for the first and second derivatives, the expansion (17) yields

$$p_{-1} = 3.5p_0 - 4.5p_1 + 2.5p_2 - 0.5p_3 + O(\Delta x^3). \tag{21}$$

Another scheme results if the centered formula (18) is used for the first derivative and the one-sided formula (9) is used for the second derivative, i.e.,

$$p_{-1} = 4p_0 - 6p_1 + 4p_2 - p_3 + O(\Delta x^3). \tag{22}$$

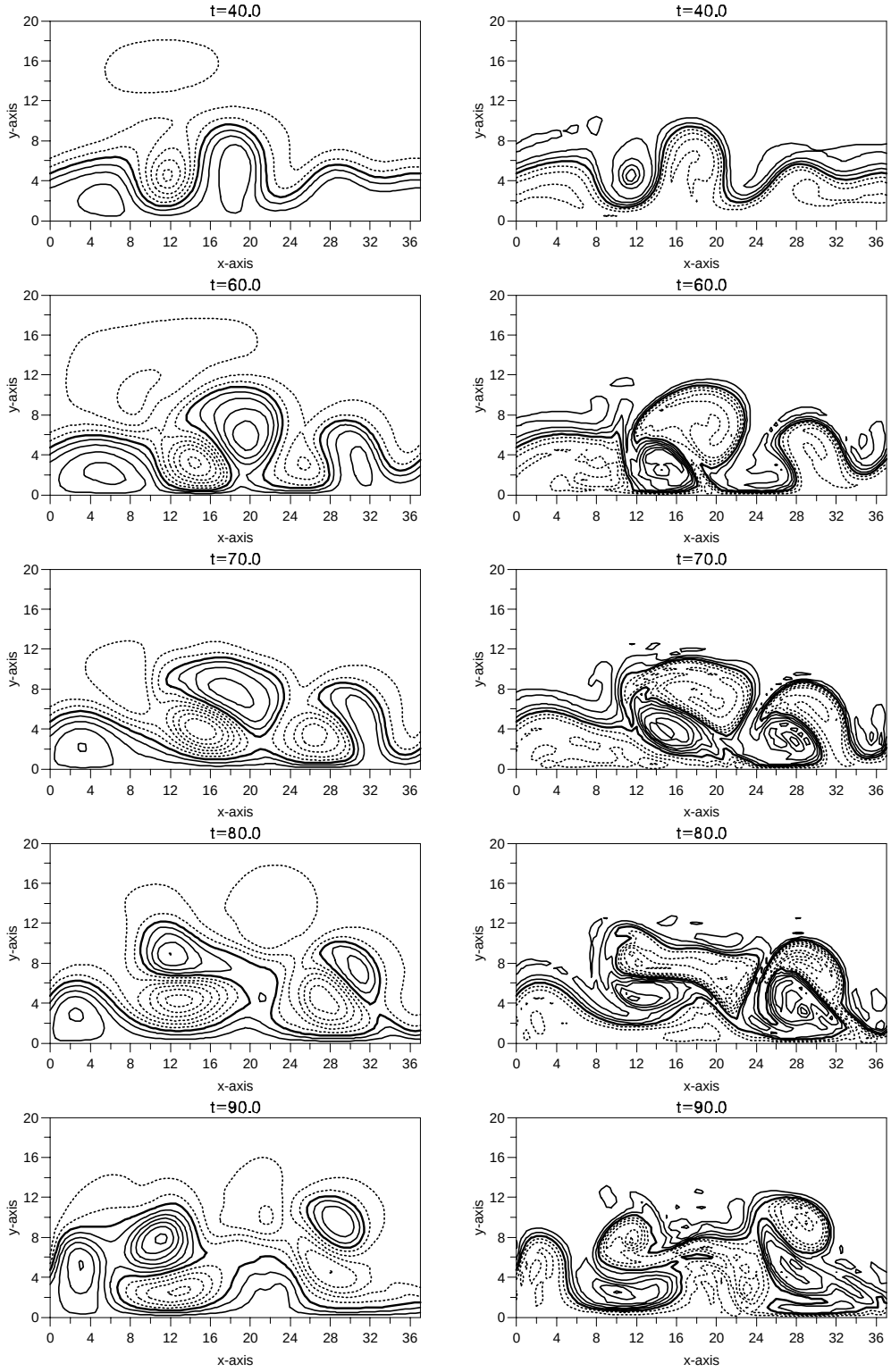

Fig. 1. The stream function (left column), and the potential vorticity (right column) for case O1.

If the one-sided formula (19) is used for the first derivative and the centered formula (20) is used for the second derivative the following scheme is found,

$$p_{-1} = 3p_0 - 3p_1 + p_2 + O(\Delta x^3), \tag{23}$$

and if only centered formulas are used, that gives a linear extrapolation formula.

All the three formulas (21–23) can be used, and they give rather similar results. However, formula (22) has proven to give slightly higher accuracy than the two others in the uniform and steady flow cases to be discussed in the next section. Formula (22) can also be derived by setting the centered and the one-sided formulas for the second order derivative equal to each other and solving for p_{-1}.

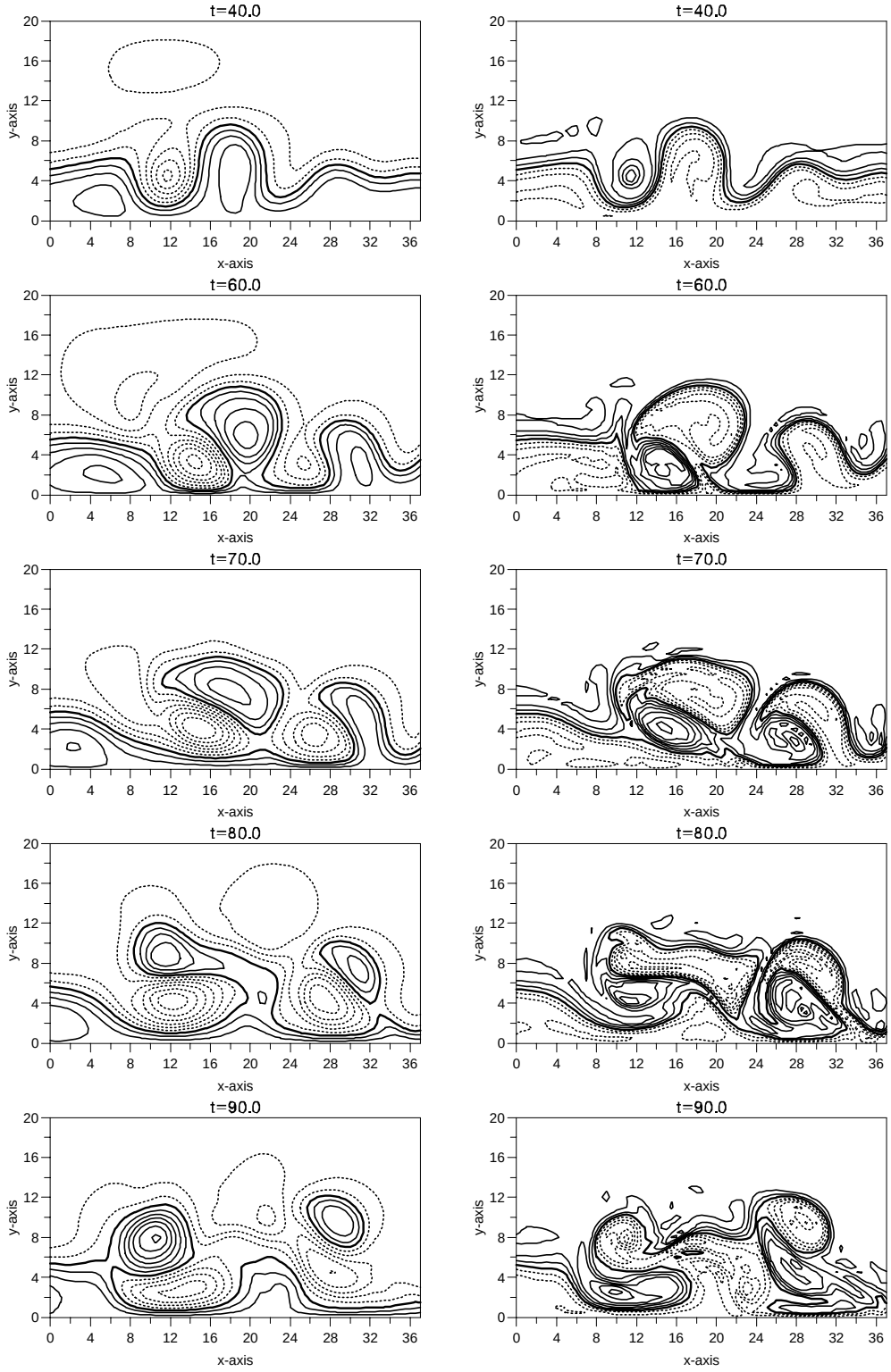

Fig. 2. The stream function (left column), and the potential vorticity (right column) for case O2.

When p_{-1} is known, the boundary conditions for the intermediate covariance functions can be estimated by advecting the covariance functions into the boundary points.

If this scheme is used also to estimate the boundary values for the final covariance functions in step 4, an instability occurs. Instead an assumption of an error covariance which is constant in time on the inflow boundaries has been used. This results in an approximate but stable method with acceptable accuracy for the error covariance evolution close to the inflow boundaries. In summary, the error covariance equation is stepped forward in the following way.

First, the boundary values of the covariance functions are stored for later use. The matrix-matrix multiplication $P_a = F_k P_k$, is calculated with the boundary error covari-

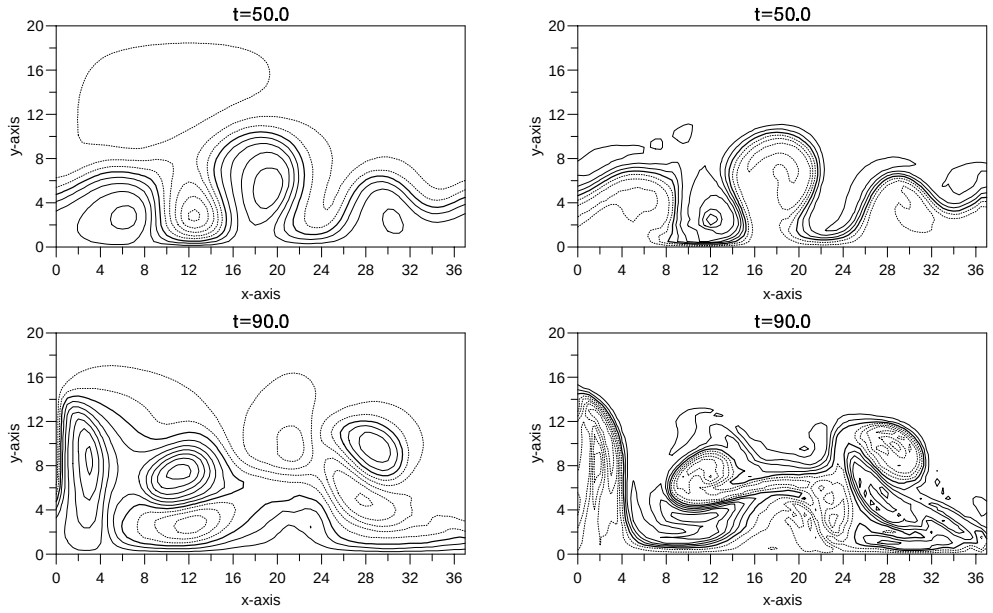

Fig. 3. The stream function (left column), and the potential vorticity (right column) for case O3.

ance vorticity estimated using the one-sided difference formula (9). The elliptic systems $LP_b = P_a$ are solved with the boundary values for the intermediate covariance functions estimated in the following way: First an estimate of the covariance functions at locations outside the boundaries is calculated using an extrapolation formula. Next, the boundary values are approximated by advecting the covariance functions in the model velocity field, using the same advection formula that is used in the ocean model. The matrix-matrix multiplication $P_c = F_k P_b^T$ is then calculated where the intermediate covariance vorticity on the boundaries is estimated using the one-sided difference formula (9). The elliptic systems $LP_d = P_c$ are solved using the stored boundary conditions from the first step above.

Symmetrization Algorithm

This is a nonsymmetrical update of the form AP_kB where $A \approx B$, and the resulting covariance matrix is only approximately symmetric. An algorithm must therefore be used to ensure symmetry. The symmetrization algorithm is based on the fact that all the columns in the updated covariance matrix P_d, corresponding to boundary points, contain covariance functions calculated from the exact covariance values that were stored from the previous time step. These columns are therefore copied to the corresponding rows of P_d. After this process, all the columns and rows in P_d that correspond to boundary points, contain the correct covariance functions. The covariance values in the interior domain are estimated using an averaging between the mirror values about the diagonal in P_d. Finally, the system noise is added, $P_{k+1} = P_d + Q_{k+1}$.

Test Runs for the Error Covariance Boundary Scheme

The following three runs are performed to examine the stability and accuracy of the boundary scheme for the error covariance equation. A uniform flow in the x direction is specified through a two-layer 25×13 domain, on a flat bottom. The boundary $x = 0$ is an inflow boundary, $x = 12$ is an outflow boundary and the two boundaries $y = 0$ and $y = 6$ are closed boundaries. At the closed boundaries free slip conditions are used, and this implies that the boundary conditions for the intermediate covariance function also must be updated there. The same method has been used for all types of boundaries.

Only the first term in the tangent linear operator (15) has been used in the following runs. However, for the cases in this section, with zero vorticity and a flat bottom, the second correction term is equal to zero. There are no conceptual problems involved in using both terms of the transition matrix with the proposed boundary scheme.

The three cases (denoted E1, E2, and E3) are all describing pure error covariance evolution in the uniform velocity field and no data are assimilated. The difference of the cases is the choice of the initial error variance field. The covariance functions are those used in Part I.

In case E1 the initial error variance is identical to one, all over the domain, and in Figure 6 the evolution of the error covariances is illustrated when using the proposed boundary scheme. When $t = 20$, i.e., after 40 time steps the error variance field is almost unchanged from the initial field. The evolution has been slightly influenced by diffusion in the advection scheme, and there is a slight error increase close to the inflow boundary and a small error decrease close to the outflow boundary. This is caused by the approximations in the boundary scheme, and further integration of the model will not change the solution at $t = 20$ which has reached a steady state. Note also that the values at the boundaries are unchanged. The shape and the amplitude of the covariance function close to the inflow boundary are almost unchanged after the time integration. In this example it is obvious that the boundary scheme gives a valid approximation for error covariance evolution.

In case E2, a slightly different example has been run, where the initial error variance is set close to zero both at the closed boundaries and at the outflow boundary. The re-

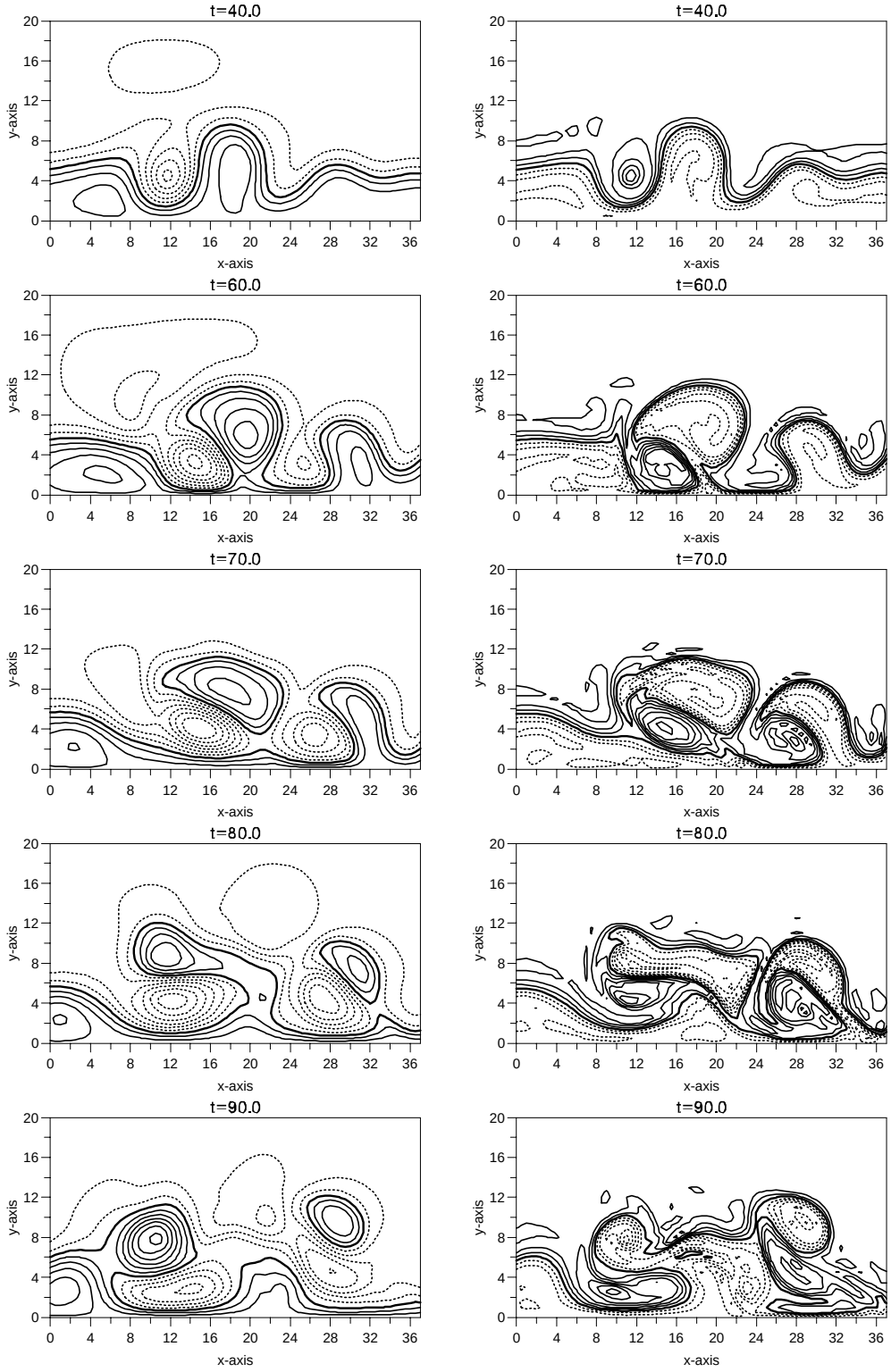

Fig. 4. The stream function (left column), and the potential vorticity (right column) for case O4.

sulting error variance field and error covariance function is shown in Figure 7. The error variance approaches a steady state where the errors are gradually decreasing towards the outflow and closed boundaries which are kept constant. The slight increase of the error right inside the inflow boundary which was found in the previous example can also be seen here, and it is also reflected in the amplitude of the covariance function. The errors should actually propagate out through the outflow boundary but that requires a radiation condition to be used for the covariance functions.

A case E3 has been run to illustrate how the estimated errors at the inflow boundary are propagating into the domain. In this case the initial errors are given low values at all the inflow, outflow, and closed boundaries (see Fig-

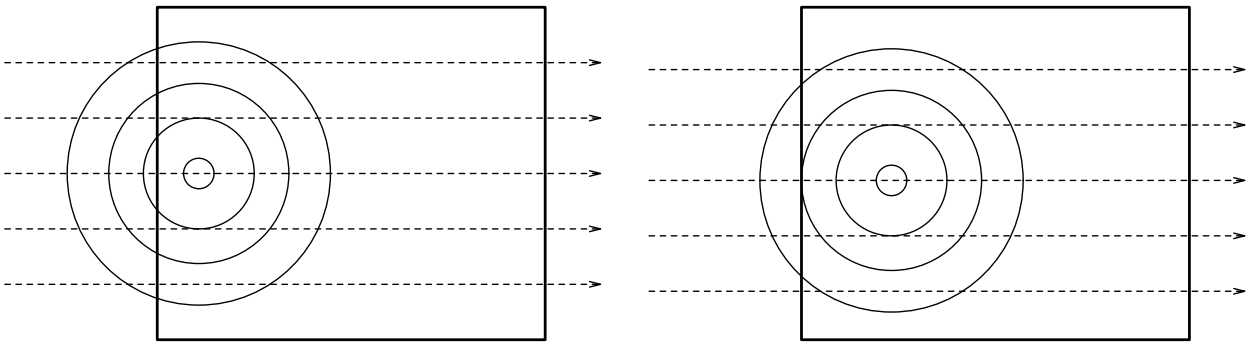

Fig. 5. (left) A covariance function close to the inflow boundary, and (right) the intermediate covariance function.

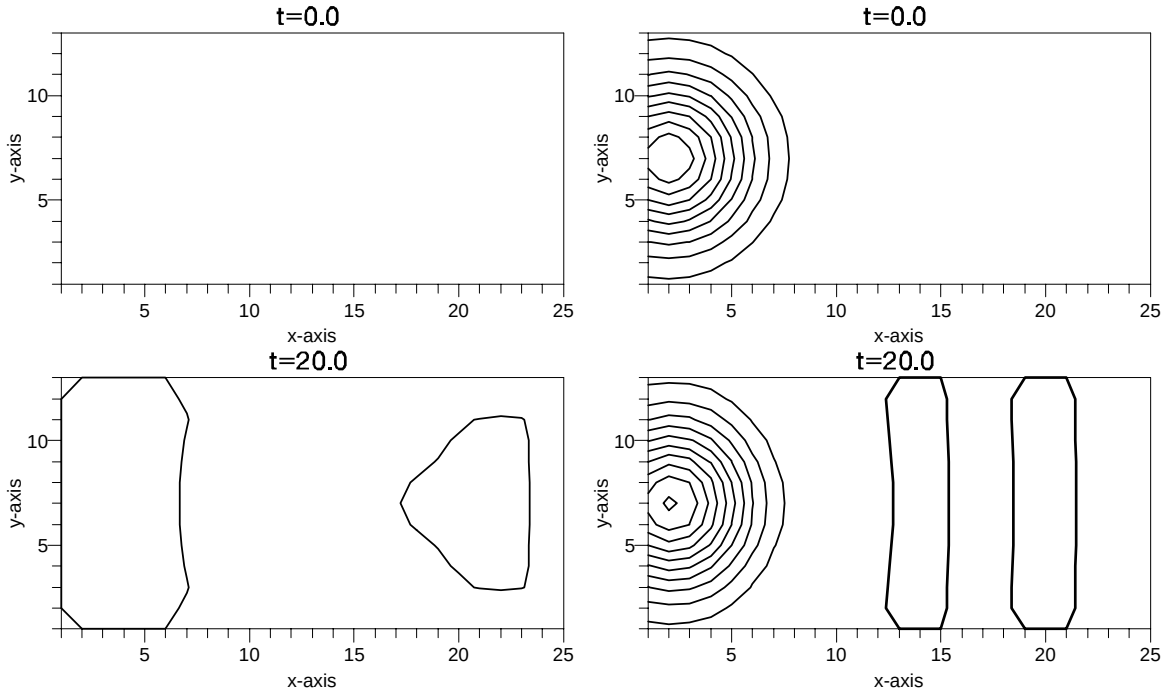

Fig. 6. Results from case E1. In the left column the error variance is shown at $t = 0$ and $t = 20$. In the right column the covariance for the stream function in grid point (1,2,7) (corresponds to $x = 0.5$ and $y = 3.0$ in the upper layer) is shown for $t = 0$ and $t = 20$. The contour interval is 0.1 in all plots.

ure 8). The low errors on the inflow boundary indicates that the solution on the inflow boundary is well known, and this information is propagating through the domain in the model velocity field. This indicates that the choice of the error variance on the inflow boundaries is crucial for the data assimilation process due to the influence it has in the interior domain.

In a data assimilation experiment one would assume a finite error variance at the inflow boundary and keep it constant in time. This is equivalent to saying that the solution on the inflow boundary contains errors, and this error is propagating into the domain. The influence of the erroneous inflow stream function is then reduced downstream, when measurements are assimilated.

A case was also run where the same boundary values were used both for the intermediate and the final covariance functions, i.e., the boundary covariance values were kept constant during a time step. However, for significant inflow this approach did not work. It introduced an error growth inside the inflow boundary with amplitudes reaching 50 times the initialized error field. These errors then propagated into the domain with the flow and corrupted the error estimates in the internal domain. Note that this method is numerically stable, and it is a pure boundary effect that causes the error growth. In some cases when there is good data coverage close to the inflow boundary, these can be used to control the boundary effect, but in general a more sophisticated method must be used.

Data Assimilation Experiment

A final test of the schemes for the boundary stream function and vorticity, and the boundary scheme which has been proposed for the error covariance evolution equation, will now be given. A simple reference case where a jet is propagating through a domain and where the dynamics are generated by the interaction between the jet and an eddy is used to generate measurements. The same physical parameters are used for the ocean model and the initial conditions as

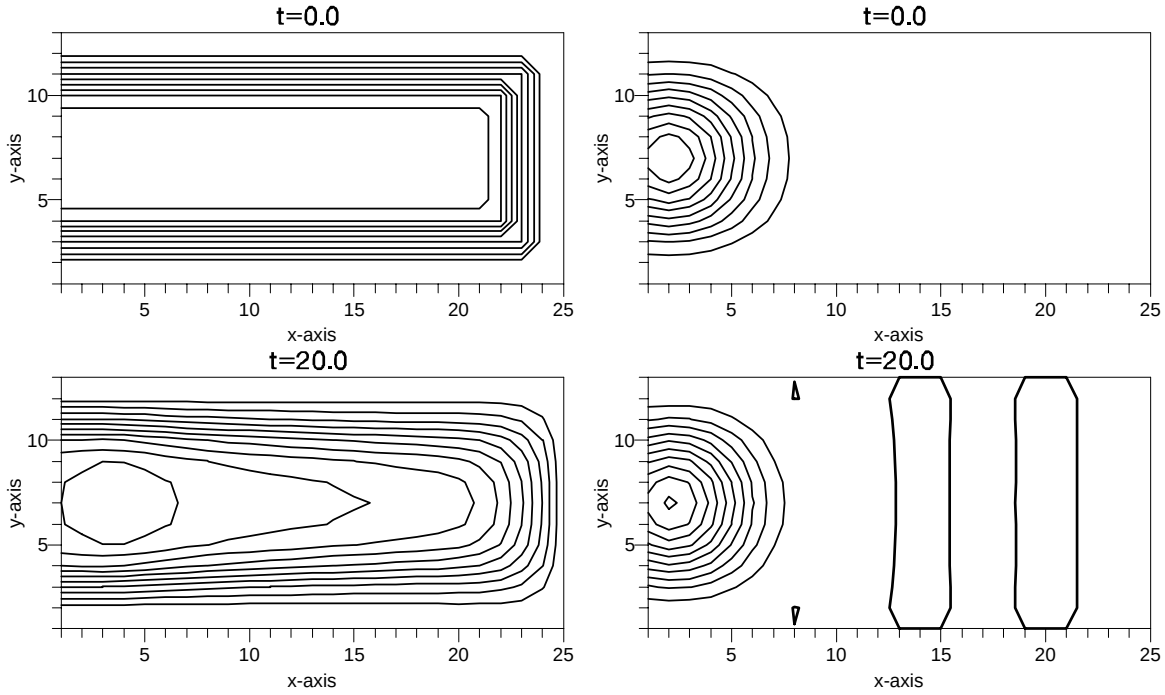

Fig. 7. Same as Figure 6 but for case E2 with zero error variance on the closed and outflow boundaries.

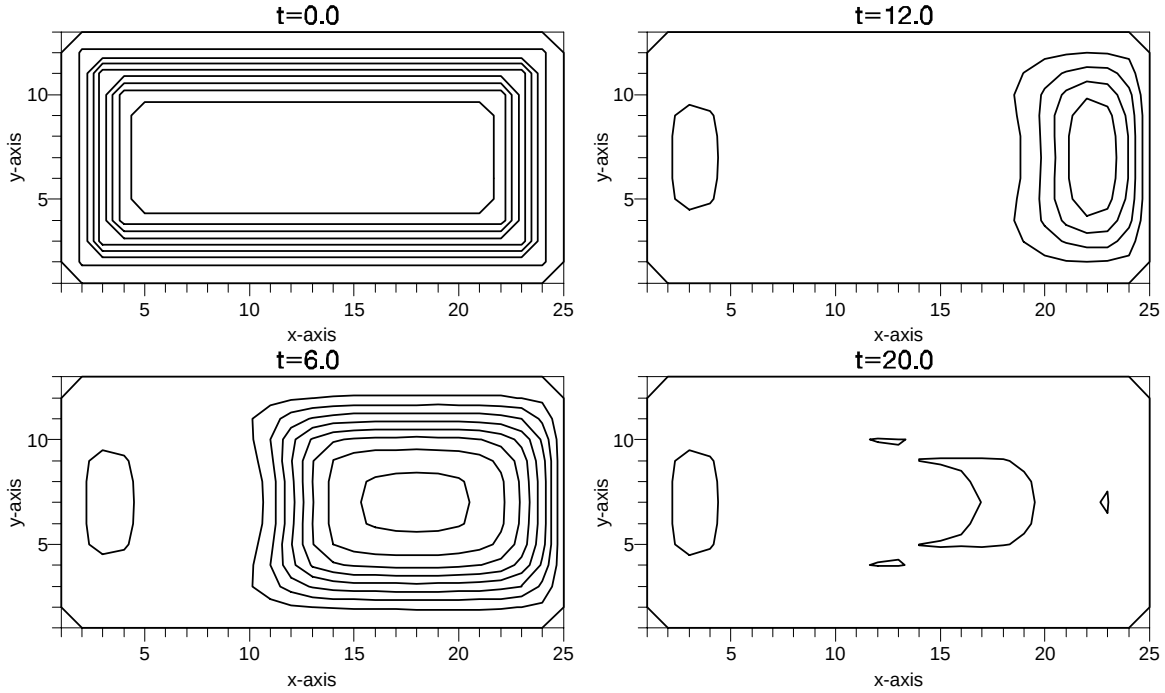

Fig. 8. Same as Figure 6 but for case E3 with low errors on the inflow boundary in addition to the closed and outflow boundaries.

was described in the test runs for the QG model, except that the locations of the eddy and the jet axis are redefined. The eddy is now initialized with the center at $(4.5, 4.5)$, and the initial jet axis is at $y = 5.0$. A smaller grid has also been used, $(27 \times 27$ in two layers). There are 1458 unknown stream function values, and the total number of unknowns in the error covariance matrix is $2,125,764$, which requires about 8.5 megabyte of storage in single precision. The bottom is sloping with increasing depth in the positive x direction, and the barotropic cyclone propagates along the bottom slope and perturbs the baroclinic jet. The first scheme, where the cross-boundary variation is neglected, has been used for the relative vorticity on the boundaries. This was a natural choice because the jet propagates almost normal to the boundary. Further, a radiation condition was used for the boundaries $x = 0$ and $x = 13$. A time series of

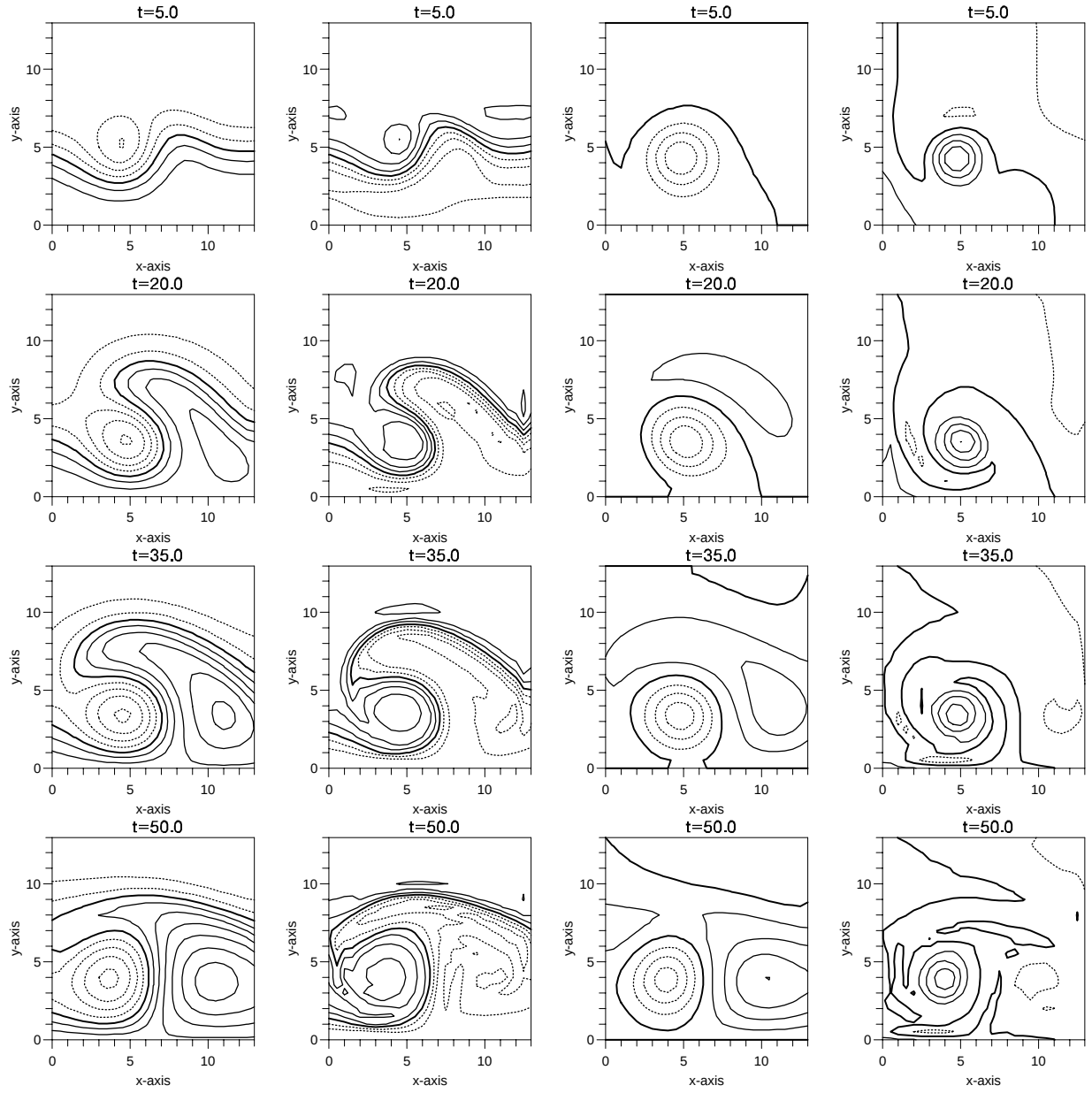

Fig. 9. Reference run: From left; stream function in layer one, vorticity in layer one, stream function in layer two, and vorticity in layer two. The contour intervals are 0.5 for both the stream function and the vorticity.

the stream function from the reference run is shown in Figure 9. It is seen how the barotropic eddy generates a strong perturbation in the upper layer jet. Note that the axis of the jet moves about 3 unit lengths on the inflow boundary. Measurements are taken at time intervals $\Delta t_{\text{obs}} = 2.5$, in 20 grid points in the upper layer. This corresponds to an extremely good data coverage, and as will be seen from the next data assimilation examples, the convergence towards the reference solution is rather fast. Note that the purpose of this experiment is to verify that the proposed boundary scheme is stable and that it works for the error covariance evolution. For this reason measurements have also been assumed to exist on the inflow boundary. Since the boundaries $y = 0$ and $y = 13$ are closed, this corresponds to flow through a channel, and the mass transport is then defined by the difference in the stream function values between the closed boundaries.

The initial error covariance matrix and the system noise is defined from the equation

$$\sigma(l_1, i_1, j_1, l_2, i_2, j_2)^2 = E(i_1, j_1)E(i_2, j_2) \times \exp\left(-\frac{||\mathbf{r}_2 - \mathbf{r}_1||_2^2}{r_h^2}\right) \exp\left(-(l_1 - l_2)^2 r_v^2\right) \quad (24)$$

which was also used in Part I.

Assimilation Experiment A

A test case is now generated where the initial stream function only includes the straight jet in the upper layer. The measurements will then have to regenerate the eddy and the perturbation in the jet. The resulting stream function, potential vorticity, and error variance field from this data

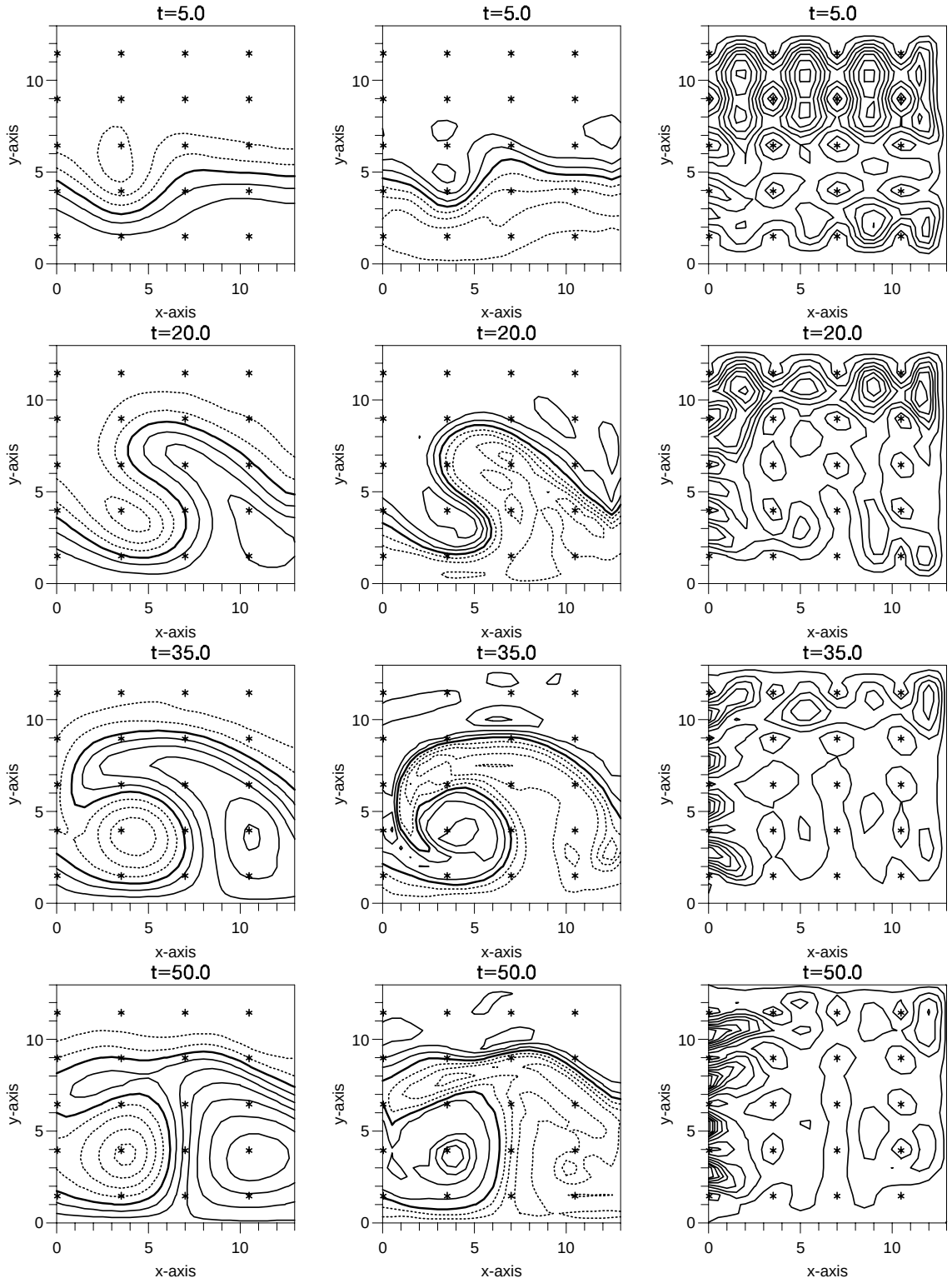

Fig. 10. Assimilation experiment A: Upper layer stream function, vorticity, and error variance field. The contour intervals are 0.5 for the stream function and the vorticity, and 0.1 for the error variances. The asterisks denote the locations of the measurements.

assimilation run is shown in the Figures 10 and 11 for the upper and lower layer, respectively.

The reference stream function in both the upper and lower layer is almost regenerated after only a few updates with the Kalman filter. The data coverage is very good in the sense that the mesoscale structures are resolved, and such an efficient data assimilation process is expected. The vorticity fields are also quite similar to the reference case and this suggests that the boundary vorticity scheme gives a realistic approximation for boundary vorticity in this case.

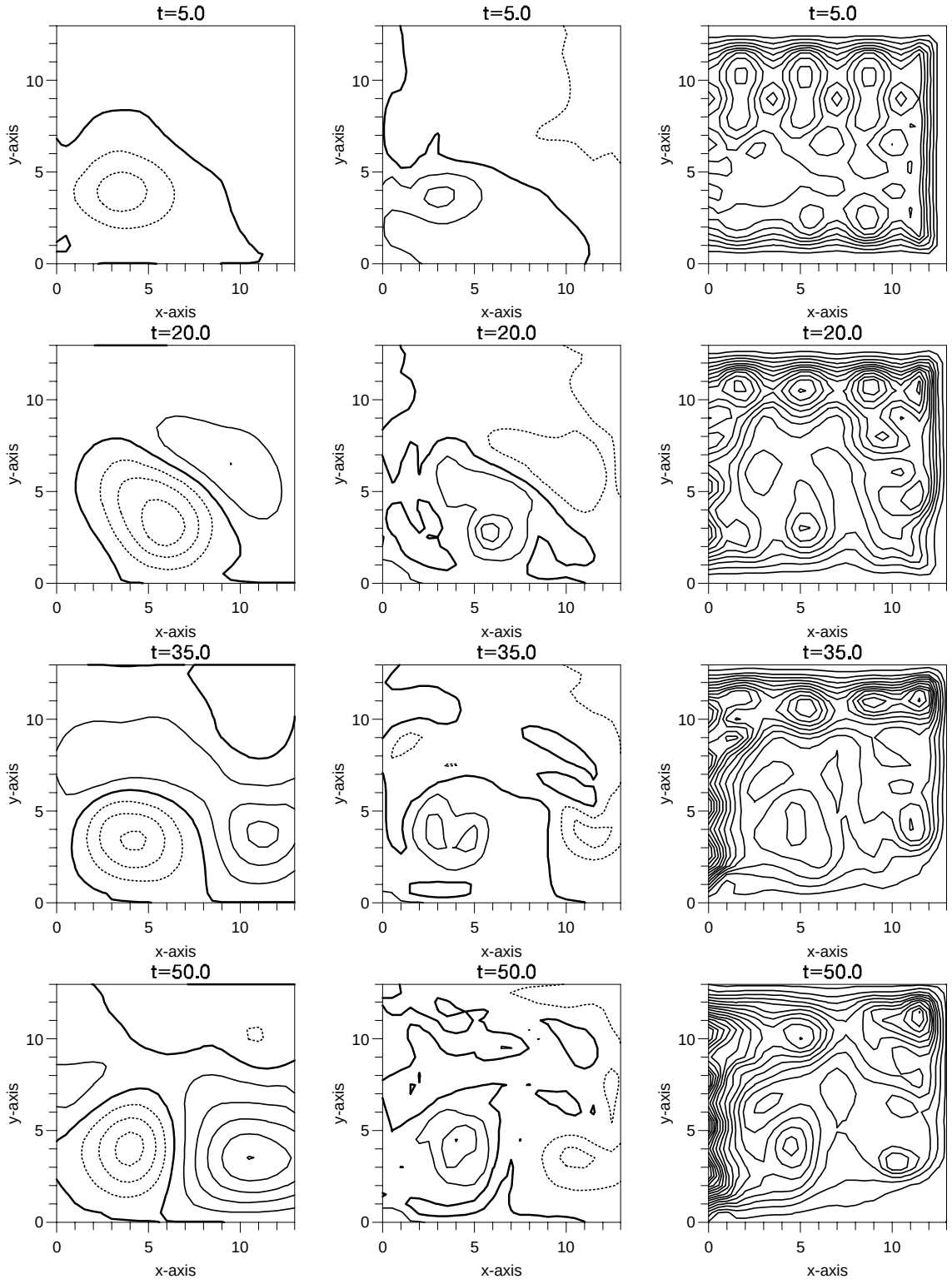

Fig. 11. Assimilation experiment A: Lower layer stream function, vorticity, and error variance field. The contour intervals are 0.5 for the stream function and the vorticity, and 0.1 for the error variances.

The initial error variance field is given with low values on the closed boundaries where the stream function is assumed to be known. These boundaries will not be influenced significantly by the measurements. This is equivalent to assuming that the fluid transport through the channel is known and constant in time. The measurements will then only be able to influence the general circulation in each layer and not the mean fluid transport. In this example the error variances are decreasing faster in the part of the domain with the strongest circulation. This is caused by the spreading

of information (low error variances), from the measurement locations by the dynamics.

The lower layer stream function is influenced by the measurements in the upper layer because a certain correlation is assumed between the layers. A value of $r_v = 0.5$ was used in the formula for the error covariance functions (24). The results show no trace of the upper layer jet in the lower layer stream function. The main reason for this is that a zero transport through the channel in the lower layer was imposed on the dynamics. However, the barotropic eddy is regenerated after only a few data updates.

Note that the initial error variance on the outflow boundary was also given a low value. This was done for numerical reasons. The boundary scheme seemed to be more sensitive to strong gradients in the error field close to the boundary, and because the errors in the internal domain are decreasing, a low value was given to the error on the outflow boundary.

Assimilation Experiment B

Here the previous case is extended to use an open boundary at $y = 13$. The experiment then simulates an open ocean along a closed coastal boundary. It is assumed that no knowledge about the circulation in the domain is available. In the upper layer a constant reference value, given from the measurements near the closed boundary, is used for the stream function all over the domain, and in the lower layer it is set to zero. In this experiment the data assimilation algorithm has to reproduce the correct fluid transport through the domain in addition to the circulation pattern. The results from the simulation are given in Figures 12 and 13. The same initial error covariance field has been used as in experiment A. From the upper layer stream function field it can be seen that the circulation soon becomes quite similar to the reference case, but it requires a few more updates than in the previous experiment. There are no measurements on or close to the two boundaries at $x = 13$ and $y = 13$, and because the initial error variance is quite low at those boundaries they are not much influenced by the measurements. However, because a radiation condition is used for the stream function, this helps to correct the boundaries by advecting information from the interior domain toward the boundary.

The lower layer stream function has in this case got a significant transport through the domain and the circulation pattern is very similar to what was found in the upper layer. This departs from the reference case and is caused by the assumed covariance between the upper and lower layer. This covariance actually determines statistically how baroclinic or barotropic the ocean is, and in this case it would probably be better to set the vertical correlation to zero because the jet is purely baroclinic. Then the data would not influence the stream function in the lower layer directly, and the model itself would have to spin up the lower layer eddy activity.

The error variance field contains some noisy structures close to the boundaries in this case, and there are also some problems in maintaining the positive definiteness of the error covariance matrix. After about $t = 35$, some occurrences of a few small negative elements appeared on the diagonal. These are caused by the nonsymmetrical update which is used in connection with the approximate boundary scheme. Such an update may lead to loss of positive definiteness after some time, and suggest that a better symmetrization algorithm which also ensures positive definiteness should be used. At present, the problem is solved by adding a small constant to all the diagonal elements every time a negative value occurs.

SUMMARY

The extended Kalman filter has been implemented for data assimilation with a nonlinear multilayer quasi-geostrophic (QG) ocean circulation model. The QG model was chosen because it is one of the simplest nonlinear models which gives a realistic description of the mesoscale ocean circulation. It includes barotropic and baroclinic instability mechanisms, and it has proven to give realistic results for the circulation on the Norwegian continental shelf [*Ikeda et al.*, 1989; *Haugan et al.*, 1991; *James*, 1991]. Two other properties also made this choice of model attractive. First, the fast inertial gravity waves have been filtered away, and this allows the use of long time steps compared to the primitive equation models, and initialization shocks or shocks generated by the assimilation of measurements are avoided. Second, the model contains only one unknown variable for each grid point, and this limits the size of the state vector and also the size of the error covariance matrix when the extended Kalman filter is used.

If the extended Kalman filter shall be a convenient tool for data assimilation, it must be possible to use it with both open and closed boundary conditions. However, this poses severe problems both for the QG model, and the error covariance evolution equation. The QG model must handle the problem with boundaries that are updated by measurements or by structures approaching the boundaries, and the error covariance equation must use an approximate boundary scheme for the open boundaries.

A discussion was given on the problem of specifying proper open boundary conditions for the QG model and the corresponding error covariance equation when the QG model is used with the extended Kalman filter for data assimilation.

First, a scheme was proposed for estimating the boundary vorticity in the ocean model. This scheme allowed the boundary stream function to be changed by measurements or a radiation condition. It was shown that a scheme, where the cross-boundary variation in the stream function was neglected, worked fine for problems where the inflow was nearly normal to the boundary. Another approach could also be used where the cross-boundary variation was approximated by a one-sided difference formula when a radiation condition was used simultaneously. The accuracy of the inflow boundary vorticity will not always be crucial in a data assimilation problem. If an approximate boundary vorticity is used, the errors of this approximation can be corrected inside the domain by the assimilation of measurements.

The problem of how to specify proper boundary values for the error covariance evolution equation was then discussed. It was found that an approximate scheme had to be used, because covariance values located outside the inflow boundaries had to be estimated by some kind of extrapolation when the intermediate covariance functions, which results from the first multiplications of the tangent linear operator with the covariance matrix, are calculated. The scheme seemed to give a good approximation for the pure error evolution experiments. An advantage of the proposed scheme is that it can be used for both open and closed boundaries,

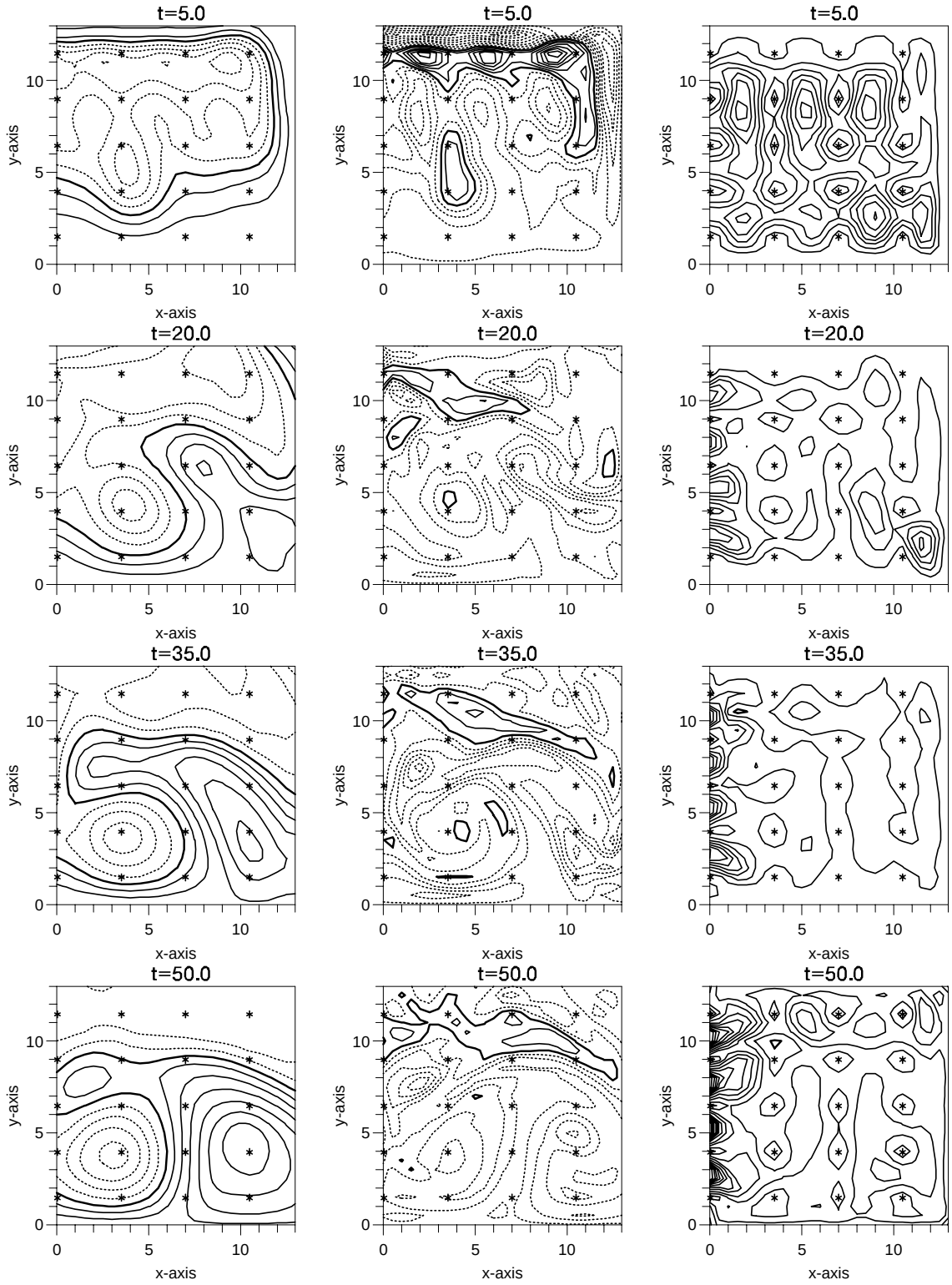

Fig. 12. Assimilation case B: Upper layer stream function, vorticity, and error variance field. The contour intervals are 0.5 for the stream function and the vorticity, and 0.1 for the error variances. The asterisks denote the locations of the measurements.

and therefore simplifies the numerical treatment considerably, both for the ocean model and the error covariance equation.

Two data assimilation experiments with synthetic data were used to illustrate the open boundary scheme. These cases proved that the open boundary scheme worked, although they pointed out a problem with loss of positive definiteness, caused by the use of a nonsymmetrical update in the approximate boundary scheme. It was therefore necessary to apply a symmetrization algorithm, which ensured

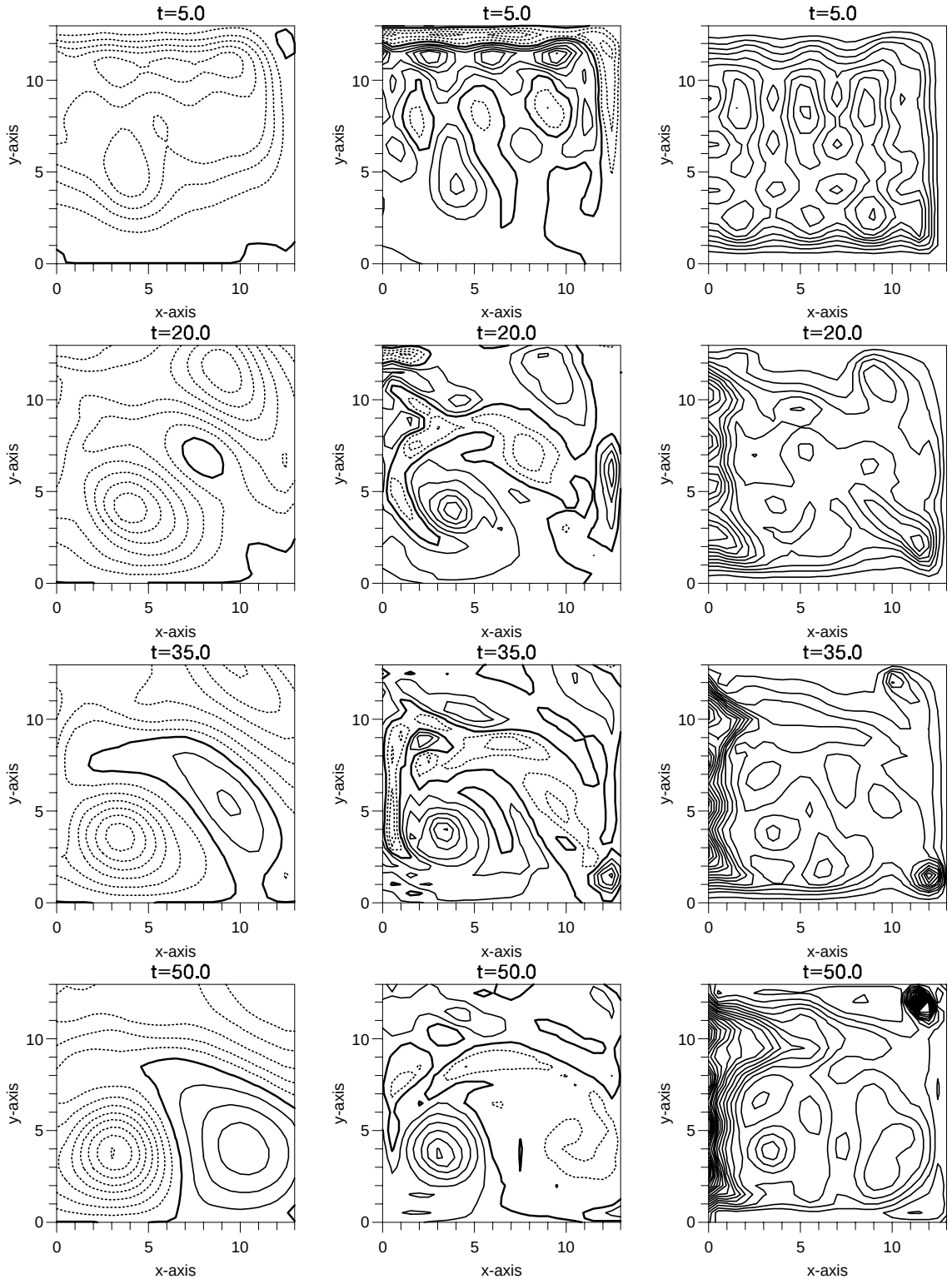

Fig. 13. Assimilation case B: Lower layer stream function, vorticity, and error variance field. The contour intervals are 0.5 for the stream function and the vorticity, and 0.1 for the error variances.

the symmetry of the covariance matrix, and for long time integrations an algorithm had to be used to keep the error covariance matrix positive definite. Here a very simple algorithm was used where a positive constant was added to the diagonal elements in the error covariance matrix.

This work also pointed at two other problems connected to data assimilation. First, how to estimate the total fluid transport through a domain or channel when using the QG model; and second, the vertical projection of surface information. It was shown that the data assimilation process

was able to regenerate the transport through a domain from data. The effect of vertical influence of the surface data has been determined by assuming a certain covariance between the upper and the lower layer. This is equivalent to assuming a statistical knowledge of how barotropic or baroclinic the ocean is in the domain of interest. With the large amount of surface information available from remote sensing satellites, this is an issue of great importance, and a more extensive treatment of the subject should be performed. A discussion of the vertical projection of surface information has been given by *Haines* [1991], in connection with a QG model.

Acknowledgments. The author would like to thank P. M. Haugan, A. H. Øien, and A. F. Bennett for valuable comments and suggestions. The work was supported by the Norwegian Research Council for Science and the Humanities.

REFERENCES

J. G. Charney, R. Fjørtoft, and J. von Neuman, Numerical integration of the barotropic vorticity equation, *Tellus, Ser. A*, *2*, 237–254, 1950.

G. Evensen, Using the extended Kalman filter with a multilayer quasi-geostrophic ocean model, *J. Geophys. Res.*, *97*(C11), 17,905–17,924, 1992.

K. Haines, A direct method for assimilating sea surface height data into ocean models with adjustment to the deep circulation, *J. Phys. Oceanogr.*, *21*, 843–868, 1991.

P. M. Haugan, G. Evensen, J. A. Johannessen, O. M. Johannessen, and L. Pettersson, Modeled and observed mesoscale circulation and wave-current refraction during the 1988 Norwegian continental shelf experiment, *J. Geophys. Res.*, *96*(C6), 10,487–10,506, 1991.

P. M. Haugan, J. A. Johannessen, K. Lygre, S. Sandven, and O. M. Johannessen, Simulation experiments of the evolution of mesoscale circulation features in the Norwegian coastal current, in *Mesoscale/Synoptic Coherent Structures in Geophysical Turbulence*, edited by J. C. J. Nihoul and B. M. Jamart, volume 50 of *Elsevier Oceanogra. Ser.*, pp. 303–313, Elsevier Science, 1989.

M. Ikeda, J. A. Johannessen, K. Lygre, and S. Sandven, A process study of mesoscale meanders and eddies in the Norwegian coastal current, *J. Phys. Oceanogr.*, *19*, 20–35, 1989.

M. Ikeda and K. Lygre, Eddy-current interactions using a two-layer quasi- geostrophic model, in *Mesoscale/Synoptic Coherent Structures in Geophysical Turbulence*, edited by J. C. J. Nihoul and B. M. Jamart, volume 50 of *Elsevier Oceanogra. Ser.*, pp. 277–291, Elsevier Science, 1989.

I. D. James, A primitive equation model simulation of eddies in the Norwegian coastal current, *J. Phys. Oceanogr.*, *21*, 893–902, 1991.

R. N. Miller, Toward the application of the Kalman filter to regional open ocean modeling, *J. Phys. Oceanogr.*, *16*, 72–86, 1986.

J. Pedlosky, *Geophysical Fluid Dynamics*, Springer–Verlag, New York, 2nd edition, 1987.

G. Evensen, Nansen Environmental and Remote Sensing Center, Edvard Griegsvei 3a, N–5037 Solheimsviken/Bergen, Norway.

(Received December 15, 1992;
revised May 18, 1993;
accepted May 18, 1993.)